

Facile Green Synthesis of Silver Nanoparticles Using *Rubus rosifolius* Linn Aqueous Fruit Extracts and Its Characterization

Marilen M. Martin and Rodolfo E. Sumayao Jr.*

Department of Chemistry, De La Salle University, Manila, Philippines

* Corresponding author. E-mail: rodolfo.sumayao@dlsu.edu.ph DOI: 10.14416/j.asep.2021.10.011

Received: 7 June 2021; Revised: 16 July 2021; Accepted: 3 August 2021; Published online: 27 October 2021

© 2022 King Mongkut's University of Technology North Bangkok. All Rights Reserved.

Abstract

Rubus rosifolius Linn is a wild raspberry found in the Philippines. The fruit extract is found to be rich in flavonoids, terpenoids, tannins, and polyphenols. It has been shown to contain interesting profiles of antioxidants and it is not previously explored as a reducing agent, specifically in the field of bio-nano research. Some of these antioxidants have been documented to have anti-cancer potential. In this study, the fruit extracts of *sampinit* were used as a reducing agent for the synthesis of silver nanoparticles (AgNPs) via a 'one-pot' facile approach. *Sampinit* aqueous fruit extract-AgNPs (SAFE-AgNPs) were synthesized by reducing silver ions using *sampinit* extract. Optical, chemical, and morphological properties of the synthesized SAFE-AgNPs were characterized. Maximal absorption of SAFE-AgNPs was observed at 415 nm which is associated with the characteristic surface plasmon resonance profile of AgNPs. SAFE-AgNPs displayed highly stable and homogeneous nanoparticles with hydrodynamic size of 85.6 ± 0.98 nm and a zeta potential of -29.5 ± 0.96 mV. HR-TEM analysis of a single crystalline image of SAFE-AgNPs corresponds to hexagonal diffraction pattern and the AgNPs were coated with soft carbon-rich materials. EDX and XRF analysis showed that SAFE-AgNPs are chiefly composed of silver (Ag) and carbon (C), where C was largely localized on the surface of AgNPs. FTIR analysis showed that SAFE-AgNPs contains key chemical functional groups associated with *sampinit*-derived phytoconstituents. Overall, the biosynthesized SAFE-AgNPs produced small size, spherical shape, and monodisperse population which can be a candidate therapeutic agent for the treatment of various diseases such as cancer.

Keywords: Green Synthesis, *Rubus rosifolius* Linn, SEM, Silver Nanoparticles, TEM

1 Introduction

The unique properties of metallic nanoparticles (NPs) have attracted keen interest of researchers and have prompted vast research on their synthesis, characterization, and application. Recent developments in NP synthesis have opened tremendous opportunities for the application of NP technology in the field of biomedical sciences and engineering. Silver NPs (AgNPs) have taken the spotlight due to their unique physical and chemical properties. AgNPs have been widely recognized for their excellent antimicrobial activities against a wide range of microorganisms which include bacteria [1], fungi [2], and parasites [3].

Generally, AgNPs can be prepared by chemical and physical methods. The traditional chemical method for the synthesis of AgNPs involves chemical reduction which requires a metal precursor (usually silver nitrate), a reducing agent, and/or stabilizing agents [4]. This synthetic method has been hampered by the inconsistent yield of NPs that are homogeneous in size and shape, as well as its associated toxicity to humans and the environment [4], [5]. Physical methods, on the other hand, do not require toxic and highly reactive chemicals and generally have rapid processing time. However, physical methods have high energy input and costly downstream processing [6]–[8]. To enhance AgNP functionality and biocompatibility, researchers

have been exploring green synthetic approaches, in which utilize biological agents such as bacteria, fungi, yeast, plant and algal extracts [4], [9]. The biological capacity to produce NPs under standard conditions requires lower capital and operating expenses and can also be implemented in nearly any setting at any scales [4], [9]. Since many biological agents can also act as surfactants and/or capping agents, biogenic NPs have the advantage of enhanced stability, biocompatibility, and reduced toxicity, which effectively mitigates its adverse health and environmental effects [9].

Recently, extracts from botanical materials such as leaves, barks, roots, and fruits were used for the biogenic synthesis of AgNPs [4]. Plants and their various anatomical parts contain proteins, pigments, secondary metabolites, and other phytoconstituents which act as reducing agents to produce nanoparticles from metal salts without producing toxic products. Some of these phytoconstituents may also serve as biosurfactants and/or stabilizing agents which promote long-term stability to metallic nanoparticles. Phytomediated synthesis of AgNPs yields nanoparticles which differed in size, morphology, stability, and bioactivity [10]. However, due to variety of biomolecules present in plant extracts, it is impossible to differentiate and observe the effect of each molecule during the reduction, nucleation, and growth steps in the nanoparticle synthesis [11].

Rubus rosifolius Linn (Figure 1), locally known as *sampinit*, is a shrub that belongs to the rose family. It can grow to a height of six feet and normally thrives in higher altitudes about 1000 to 2000 feet above sea level and can be found in the southeast Asia [12]. Its fruits are red in color when fully ripe, have hairy receptacle and are conically elongated in shape with roughly 1.5–2 cm across in length [6], [13]. Phytochemical analysis of *sampinit* confirmed the presence of different kinds of flavonoids, phenolic acids, and other bioactive compounds [14], [15]. Previous studies also showed that *sampinit* fruit extracts exhibit antimicrobial [16], antioxidant [17]–[19], anti-inflammatory [17] and anti-cancer properties [20], [21].

The need for biocompatible nanomaterials requires new nanotechnology solutions for green synthesis of AgNPs with biocompatible surfaces. Hence, surface functionalization is emphasized in this study since this may constitute a unique property



Figure 1: *Rubus rosifolius* Linn, a wild raspberry locally known as *sampinit*. It is a spiny shrub that has prickly stem belonging to the rose family. Its fruit is conically elongated in shape, has hairy receptacle and red in color.

observed only to some specific plants such as *sampinit*. To our knowledge *sampinit* has not been systematically reported as a reducing agent for the green synthesis of silver nanoparticles.

In the present study, *sampinit* aqueous fruit extracts (SAFE) were used as a reducing agent for the synthesis of AgNPs using a ‘one-pot’ approach. The SAFE-AgNPs were extensively characterized for optical properties, morphology, stability, and chemical composition. The use of SAFE-AgNPs produces desirable optical, biophysical, and structural properties.

2 Experimental

2.1 Sample collection

Rubus rosifolius Linn was harvested from Dolores, Quezon Province, Philippines with the following coordinates, 14°02’45.8” N 121°26’13.7”E. The collected fruits were authenticated and verified by the Bureau of Plant Industry, Crop Research and Production Support Division, San Andres St. Malate, Manila.

2.2 SAFE preparation

Ripe fruits were selected for aqueous extract preparation. The fruits were washed thoroughly with distilled water. The fruits were cut into small pieces and snap-frozen in liquid nitrogen. Subsequently, the fruits were

lyophilized using a freeze dryer (Heto PowerDry, ThermoFisher Scientific, Waltham, MA USA). The freeze-dried samples were ground into fine powder using a motorized blender. Powdered sample (2.0 g) was placed in an Erlenmeyer and distilled deionized water was added to a final concentration of 0.02 g/mL. The mixture was subjected to constant stirring for 30 min at room temperature (RT), protected from light. The extract was filtered using Whatmann filter no. 1 and the filtrate was stored at $-80\text{ }^{\circ}\text{C}$ until further analysis.

All chemicals were purchased from Sigma-Aldrich (St. Louis, MO USA) unless otherwise stated.

2.3 Reducing power

The reducing power of SAFE was determined using a method as described with slight modifications [22]. To 1.0 mL of 25 mg/mL SAFE, 2.5 mL of phosphate buffer (pH 6.6) and 2.5 mL of 1.0% potassium ferricyanide were added. The solution was incubated at $50\text{ }^{\circ}\text{C}$ for 20 min. Then, 2.5 mL of 10% trichloroacetic acid was added to the solution. The solution was centrifuged at 3000 rpm for 10 min at RT. The supernatant was transferred to a glass test tube and added with 2.5 mL distilled water and 0.5 mL 0.01% ferric chloride. The absorbance of the solution was measured at 700 nm using a UV-Vis spectrophotometer (Hitachi U-2900, Tokyo, Japan). Ascorbic acid (5 mg/mL) was used as a positive control. The absorbance and concentration of the sample are directly related to its reducing power [23].

2.4 SAFE-AgNP synthesis

Forty mL of 1.0 mM AgNO_3 was mixed with 3.0 mL of 2.0 mg/mL SAFE. The solution was subjected to constant stirring at $60\text{ }^{\circ}\text{C}$ for 60 min, protected from light. The pH of solution was adjusted to 6.83 using 0.1 M ammonia (NH_3). The appearance of the characteristic yellowish brown color associated with AgNP formation was monitored. The suspension was allowed to cool to RT. The AgNP suspension was centrifuged at 13,000 rpm for 15 min at RT to allow nanoparticle sedimentation. The supernatant was carefully aspirated and discarded while the pellet was washed twice with DDI H_2O . The AgNPs were lyophilized for 24 h and were stored at RT, protected from light, until further analysis.

2.5 Characterization of SAFE-AgNPs

2.5.1 UV-Vis spectrophotometry

Optical properties of SAFE-AgNPs were assessed by UV-Vis spectrophotometry. A fresh suspension of SAFE-AgNPs was subjected to wavelength scanning between 300–800 nm with a resolution of 1 nm using a UV-Vis spectrophotometer (Hitachi U-2900, Tokyo, Japan). DDI H_2O was used as a blank. The characteristic strong absorption at 415 nm was considered as a confirmation of the presence of AgNPs. The stability of SAFE-AgNPs was assessed by performing the same spectral analysis every week for 6 weeks.

2.5.2 Fourier Transform Infrared (FTIR) spectroscopy

FTIR analysis was performed for both SAFE and SAFE-AgNPs. Lyophilized samples were mixed with the potassium bromide with a ratio of 1 : 100 and pelletized. The spectrum of the sample was collected using an FTIR spectrophotometer (ThermoFisher Scientific Nicolet 6700, Waltham, MA, USA) at a resolution of 4 cm^{-1} and 64 interferogram scans in the range of $400\text{--}4000\text{ cm}^{-1}$. The various functional groups were automatically assigned using the Omnic software (ThermoFisher Scientific, Waltham, MA, USA).

2.5.3 Scanning Electron Microscopy (SEM)

Powdered SAFE-AgNP (2.0 mg) was coated with thin layer of gold and was placed on a copper grid plate. The structural morphology of SAFE-AgNPs was analysed using a scanning electron microscope (Phenom XL, Waltham, MA, USA) SEM images were captured at 26 kV and 50,000X magnification and were analysed using the ProSuite software (ThermoFisher Scientific, Waltham, MA, USA).

2.5.4 High Resolution-Transmission Electron Microscopy (HR-TEM) with Energy Dispersive X-ray Spectroscopy (EDX)

High resolution morphological analysis of SAFE-AgNPs was performed using high resolution transmission electron microscope (HR-TEM). In brief, $\sim 5\text{ }\mu\text{L}$ of aqueous suspension of SAFE-AgNPs was deposited on 200 mesh holey carbon film supported on a copper

grid and was allowed to dry at RT. The images of the SAFE-AgNPs were acquired using the JEM-2100 Plus HR-TEM (Jeol, Tokyo, Japan) with the field emission gun operating at an accelerating voltage of 200 kV.

Elemental profiling and mapping of SAFE-AgNPs were performed through locally resolved EDX microanalysis at different points HR-TEM lamellae.

2.5.5 Dynamic Light Scattering (DLS) analysis

The average hydrodynamic diameter, polydispersity index (PDI) and zeta potential of the SAFE-AgNPs were measured by DLS. An aqueous suspension of SAFE-AgNPs was sonicated (Soner 220H, Rocker Products, New Taipei City, Taiwan) at 53 KHz at 25 °C for 20 min and loaded into 10 mm polystyrene cuvettes. For zeta potential measurements, the samples were loaded into a folded zeta capillary cell. Measurements were performed at 25 °C using a fixed angle of 173° using the Zetasizer Nano ZS (Malvern Panalytical, Malvern, United Kingdom) operated at 150V. Data were analysed using the Zetasizer Ultra-Pro ZS Explorer software v1.00 (Malvern Panalytical).

3 Results and Discussion

3.1 Reducing power of SAFE (Ferric Reducing Antioxidant Potential-FRAP)

The reducing power is an estimate of the antioxidant potential of the compound [22]. Antioxidant potential is due to the reduction-oxidation (REDOX) properties of the sample. SAFE was determined to assess its ability to reduce silver ion (Ag^+) to metallic silver (Ag^0). As shown in Figure 2, SAFE displayed higher Fe^{3+} - Fe^{2+} complex absorbance than ascorbic acid (1.17 ± 0.026 and 0.81 ± 0.089 , $p < 0.05$), which indicates that SAFE has a higher reducing power compared to the potent reducing agent, ascorbic acid. The high reducing potential of SAFE is due to the presence of highly reducing phytochemicals in *sampinit* such as flavonoids and phenolics as reported in several studies [6], [15], [24]. Hence, SAFE may be considered as an effective reducing agent for AgNP synthesis. This result is consistent with the ability of *Rubus rosifolius* leaf extract to reduce Fe^{3+} complex ion to Fe^{2+} [25]. This is correlated with the antioxidant potential involving single electron transfer mechanism. The

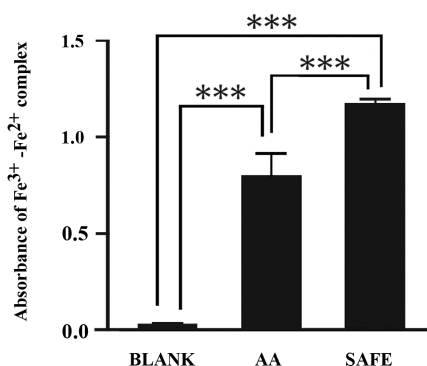


Figure 2: Reducing power (RP) of SAFE. Data are expressed as mean \pm SD of four replicates per group. *** denotes statistically significant differences ($\alpha = 0.001$). AA represents ascorbic acid.

methanol, ethyl acetate, and n-hexane leaf extracts of *R. rosifolius* gave the FRAP capacities equal to 96.50%, 82.83%, and 73.51%, respectively indicating its antioxidant potential.

3.2 SAFE-AgNP synthesis

The appearance of a yellow-brownish color upon the addition of a reducing agent to AgNO_3 has been routinely used as an indicator of AgNP formation [20], [26]. The addition of SAFE to AgNO_3 solution resulted in a change in color (yellow brown). This color change is associated with the surface plasmon excitation of AgNPs, which is the primary and most notable indication of AgNP formation [27], [28]. The yellow brown color intensified in the presence of NH_3 [Figure 3(c)]. Aside from pH adjustment, NH_3 can catalyse formation of AgNPs [29], promote nucleation and size-controlled synthesis of AgNPs [30]. Similar results for the effect of NH_3 with or without chemicals that control the size and catalyse formation of AgNPs were presented in the synthesis of AgNPs using skim rubber latex [31] and sodium citrate [32].

In this study, modification of the previously published protocols for the biosynthesis of AgNPs was performed by optimization of the parameter conditions such as the mass ratio of the SAFE to AgNO_3 , pH, temperature, and reaction time. It was observed that the higher the concentration of the fruit extract with the right concentration of the AgNO_3 used in the synthesis of AgNPs, the smaller the size of the

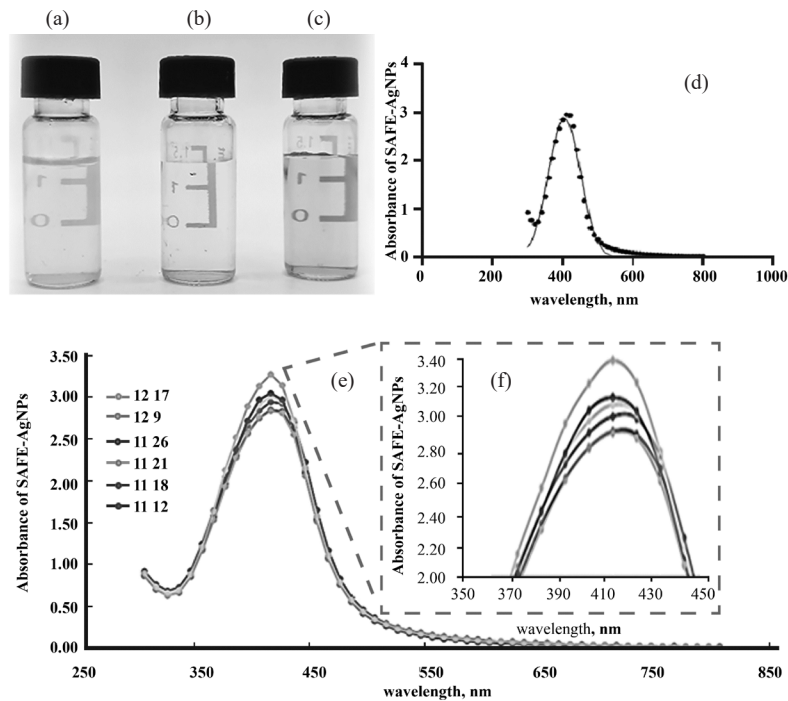


Figure 3: Monitoring of the biosynthesis of SAFE-AgNPs: (a) SAFE (20 mg/mL) added with 100 mL deionized water; (b) SAFE (20 mg/mL) added with 40 mL 1.0 mM AgNO₃; (c) SAFE (20 mg/mL) added with 40 mL 1.0 mM AgNO₃ and 0.1 mM NH₃; (d) UV-Vis spectrum of SAFE-AgNPs at 415 nm absorbance.; (e) Weekly absorbance spectra of SAFE-AgNPs showing no shift in peaks.

nanoparticles produced. The reason is that the more extract molecules that cap the surface of the AgNPs the more the growth could be controlled [33]. In this study, optimized condition was achieved at slight acidic pH 6.83. Synthesis of the small and uniform sized AgNPs could be achieved by altering the pH of the reaction mixture depending on the nature of the plant extract [34]. Slightly acidic to basic condition facilitates fast nucleation process leading to formation of smaller sized AgNPs [35]. Similar result was reported to have reached a more benign AgNPs at pH 6 [36]. The optimized temperature achieved in the biosynthesis of SAFE-AgNPs is 60 °C for an hour. As the temperature is increased the yellow brown colored solution of the AgNPs was intensified. This is due to the decomposition of the precursor salt in the reaction mixture [36]. Generally, nucleation takes place rapidly at high temperature leading to the synthesis of smaller sized AgNPs [36]. As for the reaction time, the longer the aging process the more extract molecules that adhere on the surface of the SAFE-AgNPs were formed [36].

This leads to a controllable growth of the nanoparticle [36].

3.3 Characterization of SAFE-AgNPs

UV-Vis spectroscopy is an important characterization technique to monitor the formation and stability of AgNPs in aqueous solutions [37]. AgNPs exhibit strong absorption peak between 350 and 450 nm due to the collective oscillation of free conduction band electrons of particles also known as surface plasmon resonance (SPR) phenomenon [38], [39]. UV-Vis spectral analysis of SAFE-AgNPs yielded a strong absorption peak at 415 nm [Figure 3(d)]. The intensity of the absorbance of SAFE-AgNPs at 415 nm remained strong over a period of 6 weeks [Figure 3(e)]. The periodic observation of SAFE-AgNPs during the storage period of 6 weeks showed almost consistent absorption spectrum without shift in the peak wavelength which indicate the stability of SAFE-AgNPs. The results agree with the previous study where the proanthocyanidins-

functionalized AgNPs revealed stability during the storage of longer than a month since no obvious changes in the UV absorption spectrum were observed [28]. Similar results were reported with the preparation of AgNPs from the inflorescence of *Cocos nucifera* [12] and from the peel of *Punica granatum* [17] with longer period of storage, 2 and 4 months, respectively where no variation on the spectral characteristics on the absorption spectra was observed.

3.4 Structural and morphological properties of SAFE-AgNPs

Dynamic Light Scattering (DLS) analysis was performed to determine the size distribution profile, as well as the polydispersity index (PDI), of SAFE-AgNPs. There were 2 peaks, peak 1 and peak 2, detected in the particle size distribution analysis where peak 2 represents larger particle size SAFE-AgNPs. Majority of the size was represented by peak 2. This might be due to the intensity of the light scattered by the larger particle sized SAFE-AgNPs which totally conceals the signal from smaller ones [40]. Hence, the average hydrodynamic size of SAFE-AgNPs was 85.6 ± 0.98 nm [Figure 4(a)].

The zeta potential is an important parameter used to evaluate the surface charge of micro- or nanoparticles in colloidal dispersions, which is associated with their stability. The average zeta potential value obtained for SAFE-AgNPs was -29.5 ± 0.96 mV [Figure 4(b)]. Zeta potential values above +25 mV and below -25 mV have high degree of stability [41]. Therefore, SAFE-AgNPs are considered highly stable. Several reports demonstrated similar zeta potential values below -25 mV for AgNPs. *Fumaria parviflora* extract mediated biogenic synthesis of AgNPs obtained a zeta potential value of -29.6 mV, which caused greater stability and prevent agglomeration for the synthesized AgNPs [36]. A study of the green tea extract mediated biogenic synthesis of silver nanoparticles obtained a negatively charged zetapotential value, -39.6 mV, which suggested not only high stability of the biosynthesized AgNPs but also the presence of the active organic phytoconstituent, polyphenol, present in green tea [21].

The PDI was measured to determine the size population distribution of SAFE-AgNPs. A PDI value equal to 0 represents a monodisperse distribution and a PDI value equal to 1 represents a polydispersed

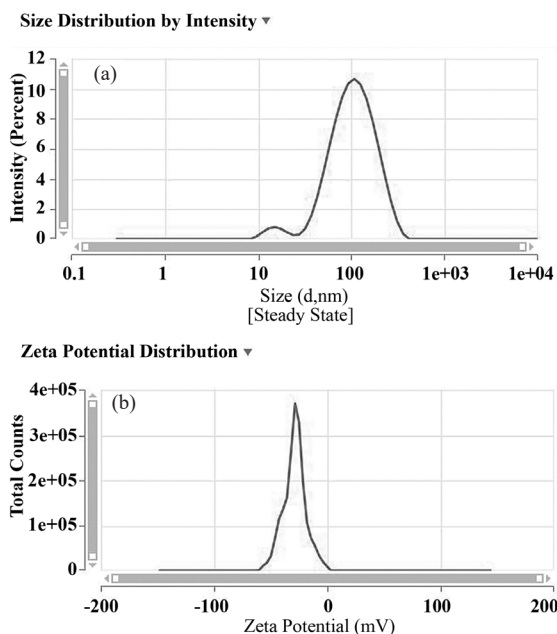


Figure 4: (a) Particle size distribution profile and (b) Zeta Potential distribution profile of SAFE-AgNPs.

distribution [19]. The average PDI obtained for SAFE-AgNPs was 0.266 ± 0.0097 , which indicates that SAFE-AgNPs are relatively homogeneous [40]. Overall, the results were in good agreement with the biogenically synthesized AgNPs from green tea and pomegranate peel extracts where PDI values obtained were 0.28 and 0.25, respectively indicating monodisperse population for both AgNPs [21], [42].

SEM was performed to establish the surface morphology, size, and shape of the SAFE-AgNPs. The SEM images of SAFE-AgNPs revealed clusters of quasi-spherical nanoparticles with sizes ranging from 33.3 to 59.2 nm [Figure 5(a) and (b)]. SEM images revealed sizes of nanoparticles which are quite smaller than the sizes obtained in DLS. This might be due to the aggregation of several nanoparticles which is often detected as single particles by DLS [43]. In addition, the increased size of the synthesized AgNPs as determined by DLS may be due to the hydrated capping agents [44] and solvation effects. The SAFE-AgNPs used in DLS technique is in colloidal solution. The size of the SAFE-AgNPs is not only determined by the metallic core but also by the other substances that adhered on the surface of the AgNPs [40]. In addition, the thickness of electrical double layer might also add up to the size

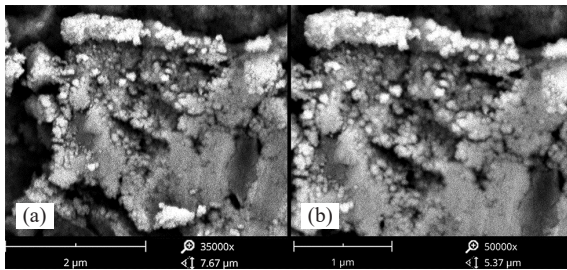


Figure 5: SEM micrograph of SAFE-AgNPs showing clusters of quasi-spherical shapes. (a) x35k magnification and (b) x50k magnification.

of the SAFE-AgNPs. The thickness of the electrical double layer depends on the substances present in the colloid and the biomolecules that capped the AgNPs [40]. Similar results were obtained in the biosynthesized AgNPs using *Matricaria chamomilla* flower extract where the sizes of AgNP-1 measured using SEM and DLS, were 70 nm and 125 nm, respectively [45]. For AgNP-2, the sizes measured using SEM and DLS were 52 nm and 105 nm, respectively [45].

A more detailed structural analysis of SAFE-AgNPs was performed using HR-TEM. Consistent with SEM analysis, HR image of SAFE-AgNP crystal structure revealed a uniformly spherical-shaped nanoparticles with an approximate size of <50 nm [Figure 6(a) and (b)]. The atomic planes of a single crystalline silver are visible from the HR lattice image of an individual SAFE-AgNP [Figure 6(c)]. The diffraction patterns in the image correspond to a hexagonal structure which was previously reported for AgNPs [46], [47]. Interestingly, an HR image of a single crystalline AgNP revealed that it is uniformly coated with a soft material, which could possibly be the phytoconstituents of *sampinit* acting as capping agents to stabilize the SAFE-AgNPs.

EDX spectroscopy was performed along with HR-TEM to confirm the elemental distribution in SAFE-AgNPs [Figure 7(d)]. EDX point mapping of SAFE-AgNPs revealed a strong signal for Ag and was mainly localized in the core domain of AgNPs (green) [Figure 7(b)]. Interestingly, carbon (C) formed a huge component of the SAFE-AgNPs and was largely diffused across the surface of the AgNPs (red) [Figure 7(c)]. The abundance of C on the surface of SAFE-AgNPs indicates that the soft materials that coat the surface of AgNPs observed in the HR-TEM image

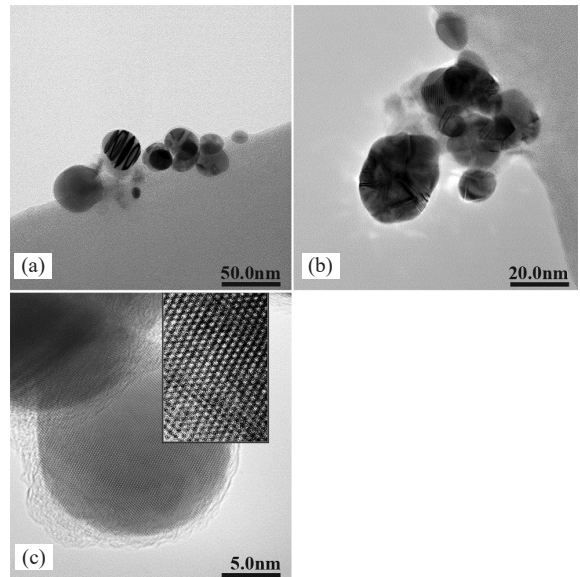


Figure 6: High resolution transmission electron microscopy bright field (HRTEM – BF) image of SAFE-AgNPs at (a) x100k magnification and (b) x150 magnification. (c) A single crystallized AgNP covered with organic phytoconstituents present in SAFE, and the inset shows the diffraction pattern corresponding to the hexagonal crystallographic planes of SAFE-AgNPs.

of a single crystalline AgNP were indeed *sampinit*-derived organic phytoconstituents. Consistent with these findings, the EDX atomic emission spectrum also revealed strong signals from Ag and C at ~3.0 keV and ~0.3 keV [Figure 7(d)], respectively, which further supports the *sampinit*-mediated capping of AgNPs, which may have promoted the long-term stabilization of SAFE-AgNPs.

3.5 Chemical composition of SAFE-AgNPs

X-ray fluorescence (XRF) spectroscopy analysis was performed for complementary elemental analysis of SAFE-AgNPs. The XRF emission spectra of SAFE-AgNPs revealed two strong signals at ~3.0 and 21 keV (blue and yellow peaks, respectively) (Figure 8), which is indicative of metallic silver. Ag metal accounts for 42.5% of SAFE-AgNPs (data not shown). The amount of silver obtained in SEM-EDX is higher compared to XRF since it is the dried purified form of AgNP that was measured in the analysis whereas, in

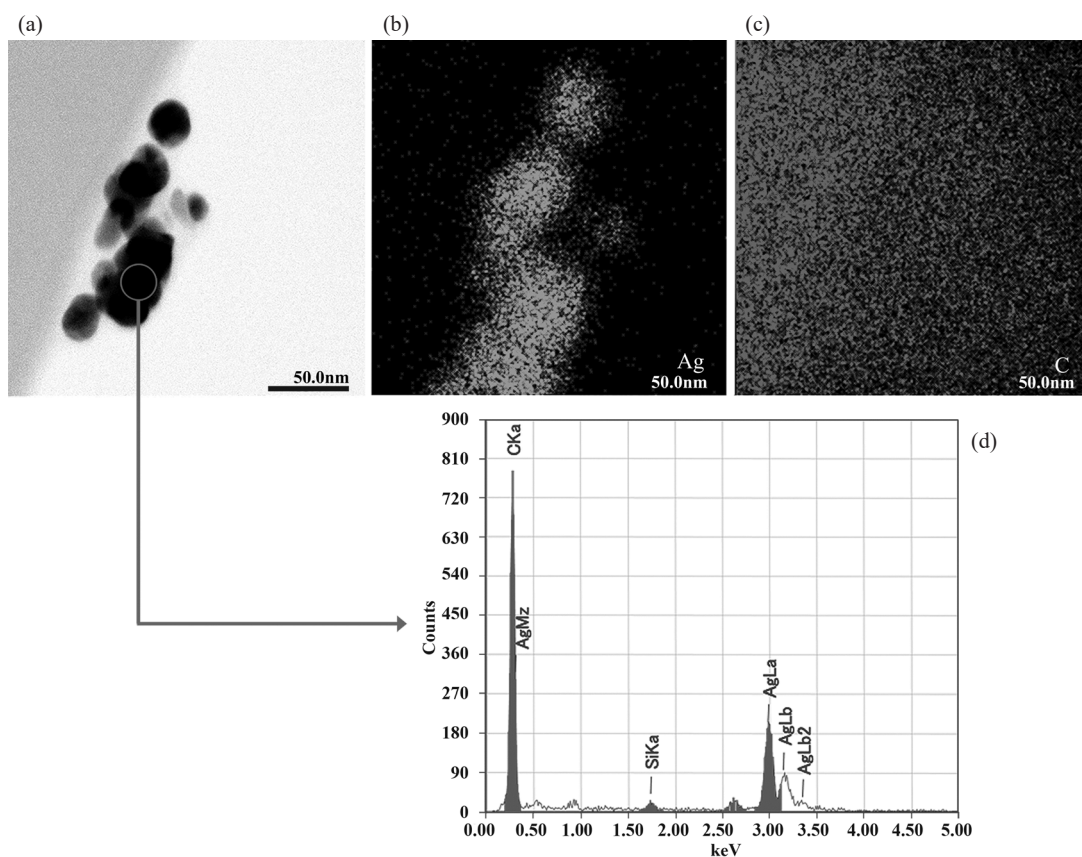


Figure 7: Scanning transmission electron microscopy (STEM)/Energy dispersive X-ray (EDX) Mapping of SAFE-AgNPs. (a) The figure displays a bright field (BF) image of dark SAFE-AgNPs on a light background. (b) The figure shows the energy dispersive mapping of silver characteristic x-ray which affirms its distribution in SAFE-AgNPs. (c) The image shows large component of carbon (in SAFE-AgNPs) surrounding the nanoparticles. (d) EDX spectrum of SAFE-AgNPs.

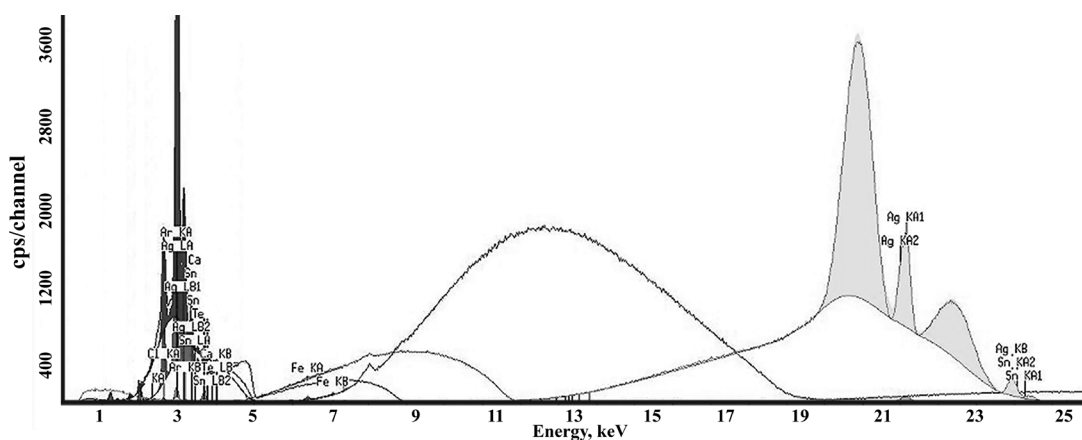


Figure 8: Elemental profile of SAFE-AgNPs determined by X-ray Fluorescence (XRF) spectroscopy.

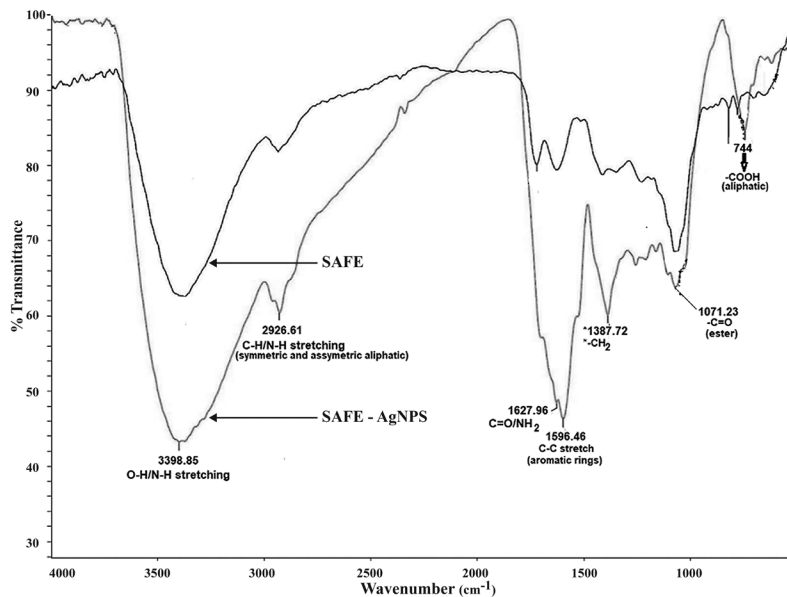


Figure 9: Overlaid FTIR spectra of SAFE and SAFE-AgNP.

XRF it is the AgNP suspension that was used. Possibly, presence of some other bioconstituents might still be involved in the analysis. Overall, these results corroborates the reduction capability of *sampinit*-derived phytoconstituents in the formation of high-yield AgNPs.

Fourier-transform infrared (FTIR) spectroscopy was performed to determine the chemical functional groups present in SAFE-AgNPs. The FTIR spectrum of SAFE-AgNPs strongly matched the spectrum of SAFE, which indicates that most of the SAFE-derived chemical compounds were successfully incorporated into the AgNPs (Figure 9). The strong broad band obtained between 3300–3500 cm^{-1} is associated with the hydroxyl and amine groups. The distinctive bands at 3396.85 cm^{-1} and 3374.06 cm^{-1} are characteristic of O-H and N-H stretching vibrations of hydroxyl and amines groups, respectively, where N-H is characterized by lower wave numbers than that of the O-H [48], [49]. These –OH groups may be associated with the polyphenolic compounds, while the –NH groups may be associated with the primary and secondary amines in amino acids and peptides present in SAFE [48]. The absorbance bands at 2926.61, 1627.96 and 1596.46 cm^{-1} are attributed to the symmetric and asymmetric aliphatic C–H and N–H stretching vibrations, to C=O or amide groups and to C–C stretch in aromatic rings of the flavonoids, polyphenols and terpenoids, respectively

[50], [51]. The bands observed observed at 1387.72 and 1256.28 cm^{-1} in SAFE-AgNPs correspond to the CH₂ stretching bend, whereas the peak at 1071.23 cm^{-1} is attributed to –C=O stretching vibration of ester groups. Lastly, the band that appeared at 744.332 cm^{-1} is associated with the aliphatic carboxylic acid. A slight shift in the absorption band at 3398.85 cm^{-1} in SAFE-AgNPs may be attributed to the multiple hydrogen bonding between the various functional groups in SAFE which, in turn, could have facilitated the stabilization of SAFE-AgNPs [16]. Furthermore, the appearance of the absorption band at 1161.73 cm^{-1} and 1105.48 cm^{-1} in SAFE-AgNPs may be associated with the shift of the deformation vibration of –OH groups, which suggests involvement of –OH groups in the bioreduction process of Ag⁺ to Ag⁰ [48].

Overall, the various functional groups detected by FTIR revealed the chemical diversity of *sampinit*-derived extract which may have aided the successful bioreduction of Ag⁺ to Ag⁰. The presence of active functional groups such as alcohol, phenol, secondary amines, amides, and carbonyl groups in SAFE-AgNPs may be attributed to the various *sampinit*-derived metabolites such as polyphenols, flavonoids, tannins, and proteins/peptides [23], [50]. These organic constituents in *sampinit* may have also adhered on the surface of AgNPs, serving as a capping agent, which accounts

for the long term stabilization of SAFE-AgNPs and prevention of their agglomeration. This is supported by a plethora of studies that utilized various plant materials or fruit extracts as reducing agents for the biogenic synthesis of AgNPs [51]–[53].

There are some studies reported on the successful synthesis of AgNPs using different *Rubus* species. Most of them reported the preparation of extract by washing, grinding, heating the samples either by regular heating [54] or via microwave [55]. Finally, heated samples are allowed to cool and filtered. In this study, same steps were performed but with the addition of snap-freezing the samples with liquid nitrogen prior to lyophilization. These additional steps were done to avoid dehydration and to preserve the samples. For the synthesis of SAFE-AgNPs, after the extraction of SAFE, it was again subjected to lyophilization to get the exact concentration of SAFE to be added to AgNO_3 . Then, AgNO_3 was added drop by drop to the extract until the formation of AgNPs. This part of the synthesis is crucial to the formation of the desirable properties of SAFE-AgNPs. Several studies had successfully synthesized AgNPs from *Rubus* species [55], [56] but none had reported to the best of our knowledge the modifications made in this study. Furthermore, the use of any *Rubus* species was able to reduce Ag^+ to Ag^0 but only *Rubus rosifolius linn* gave a stable SAFE-AgNPs with no shift in peak wavelengths within the storage period of 6 weeks.

With all the several characterization techniques performed, significant results were obtained. Hence, mechanism for the formation of stable SAFE-AgNPs is proposed. Reduction-oxidation, REDOX, reaction involves the reduction of Ag^+ to Ag^0 . An electron is gained by silver from the $-\text{OH}$ ion present in flavonoids and polyphenols, which are the active phytoconstituents present in SAFE as confirmed by the FTIR results. These phytochemicals react with silver nitrate to form the metallic silver. The $-\text{OH}$ in polyphenols reacts with Ag^+ reducing it to AgNPs (Figure 10). The biosynthesized SAFE-AgNPs was stabilized by capping the surface of the SAFE-AgNPs with the SAFE secondary metabolites as corroborated by the HR-TEM results. The capping of the secondary metabolites in SAFE prevents it from agglomeration. Furthermore, electrostatic stabilization was believed to achieve due to the coordination of the anionic species such as the OH^- to silver nanoparticles.

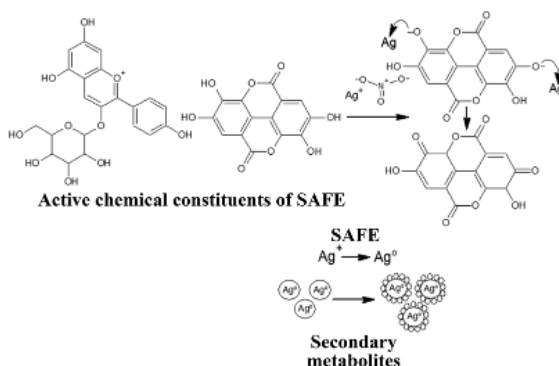


Figure 10: Proposed mechanism for the formation of SAFE-AgNPs. The reduction of Ag^+ to Ag^0 involves REDOX reaction.

4 Conclusions

In this study, the conjugation of AgNPs with *sampinit* aqueous fruit extract (SAFE) was demonstrated through a simple one pot synthesis. The developed green process can be used as an alternative approach to conventional methods in synthesizing biogenic silver nanoparticles. The active phytoconstituents present in SAFE as detected by FTIR may have aided the successful bioreduction of Ag^+ to Ag^0 and the long term stabilization of SAFE-AgNPs. Its ability to effectively reduce Ag^+ to AgNP is complemented by its high reducing power. Overall, the synthesized SAFE-AgNPs having spherical particles of <50 nm in size, a PDI value of 0.266 ± 0.0097 , and a zeta potential value of $-29.5 \text{ mV} \pm 0.96$ are remarkable characteristics and considered good attributes for effective nanocarriers.

Acknowledgements

The authors would like to extend their gratitude to Dr. Maria Carmen Tan (DLSU Chemistry Department Instrument Laboratory) and Mr. Mark Mangogtong (DKSH Philippines) for their technical assistance and to the DLSU Research Fellowship Program for the financial support.

References

- [1] S. Sadhasivam, P. Shanmugam, and K. S. Yun, "Biosynthesis of silver nanoparticles by *Streptomyces hygroscopicus* and antimicrobial

- activity against medically important pathogenic microorganisms,” *Colloids Surfaces B Biointerfaces*, vol. 81, no. 1, pp. 358–362, Jul. 2010, doi: 10.1016/j.colsurfb.2010.07.036.
- [2] J. M. Kobashigawa, C. A. Robles, M. L. Martínez Ricci, and C. C. Carmarán, “Influence of strong bases on the synthesis of silver nanoparticles (AgNPs) using the ligninolytic fungi *Trametes trogii*,” *Saudi Journal of Biological Sciences*, vol. 26, no. 7, pp. 1331–1337, 2019, doi: 10.1016/j.sjbs.2018.09.006.
- [3] A. Jaganathan, K. Murugan, C. Panneerselvam, P. Madhiyazhagan, D. Dinesh, C. Vadivalagan, A. T. Aziz, B. Chandramohan, U. Suresh, R. Rajaganesh, J. Subramaniam, M. Nicoletti, A. Higuchi, A. A. Alarfaj, M. A. Munusamy, S. Kumar, and G. Benelli, “Earthworm-mediated synthesis of silver nanoparticles: A potent tool against hepatocellular carcinoma, *Plasmodium falciparum* parasites and malaria mosquitoes,” *International Journal of Parasitology*, vol. 65, no. 3, pp. 276–284, Feb. 2016, doi: 10.1016/j.parint.2016.02.003.
- [4] K. S. Siddiqi, A. Husen, and R. A. K. Rao, “A review on biosynthesis of silver nanoparticles and their biocidal properties,” *Journal of Nanobiotechnology*, vol. 16, no. 14, 2018, doi: 10.1186/s12951-018-0334-5.
- [5] N. Kulkarni and U. Muddapur, “Biosynthesis of metal nanoparticles: A review,” *Journal of Nanotechnology*, vol. 2014, May 2014, doi: 10.1155/2014/510246.
- [6] T. F. Campbell, J. McKenzie, J. A. Murray, R. Delgoda, and C. S. Bowen-Forbes, “*Rubus rosifolius* varieties as antioxidant and potential chemopreventive agents,” *Journal of Functional Foods*, vol. 37, pp. 49–57, Jul. 2017, doi: 10.1016/j.jff.2017.07.040.
- [7] S. K. Srikar, D. D. Giri, D. B. Pal, P. K. Mishra, and S. N. Upadhyay, “Green synthesis of silver nanoparticles: A review,” *Green and Sustainable Chemistry*, vol. 6, pp. 34–56, Feb. 2016, doi: 10.4236/gsc.2016.61004.
- [8] S. Fahimirad, F. Ajalloueian, and M. Ghorbanpour, “Synthesis and therapeutic potential of silver nanomaterials derived from plant extracts,” *Ecotoxicology and Environmental Safety*, vol. 168, pp. 260–278, Jan. 2019, doi: 10.1016/j.ecoenv.2018.10.017.
- [9] A. Schröfel, G. Kratošová, I. Šafařík, M. Šafaříková, I. Raška, and L. M. Shor, “Applications of biosynthesized metallic nanoparticles - A review,” *Acta Biomaterialia*, vol. 10, no. 10, pp. 4023–4042, May 2014.
- [10] P. Rauwel, S. Küünal, S. Ferdov, and E. Rauwel, “A review on the green synthesis of silver nanoparticles and their morphologies studied via TEM,” *Advances in Material Science and Engineering*, vol. 2015, Aug. 2014, doi: 10.1155/2015/682749.
- [11] G. S. Karatoprak, G. Aydin, B. Altinsoy, C. Altinkaynak, M. Kosar, and I. Ocoy, “The Effect of *Pelargonium endlicherianum* Fenzl. root extracts on formation of nanoparticles and their antimicrobial activities,” *Enzyme and Microbial Technology*, vol. 97, pp. 21–26, Oct. 2016, doi: 10.1016/j.enzmtec.2016.10.019.
- [12] R. Mariselvam, A. J. A. Ranjitsingh, A. Usha Raja Nanthini, K. Kalirajan, C. Padmalatha, and P. Mosae Selvakumar, “Green synthesis of silver nanoparticles from the extract of the inflorescence of *Cocos nucifera* (Family: Arecaceae) for enhanced antibacterial activity,” *Spectrochimica Acta - Part A Molecular and Biomolecular Spectroscopy*, vol. 129, pp. 537–541, Apr. 2014, doi: 10.1016/j.saa.2014.03.066.
- [13] V. T. P. Vinod, P. Saravanan, B. Sreedhar, D. K. Devi, and R. B. Sashidhar, “A facile synthesis and characterization of Ag, Au and Pt nanoparticles using a natural hydrocolloid gum kondagogu (*Cochlospermum gossypium*),” *Colloids Surfaces B Biointerfaces*, vol. 83, no. 2, pp. 291–298, 2011, doi: 10.1016/j.colsurfb.2010.11.035.
- [14] H. Amanda, A. Santoni, and D. Darwis, “Extraction and simple characterization of anthocyanin compounds from *Rubus rosifolius* Sm fruit,” *Journal of Chemical and Pharmaceutical Research*, vol. 7, no. 4, pp. 873–878, 2015.
- [15] C. S. Bowen-Forbes, Y. Zhang, and M. G. Nair, “Anthocyanin content, antioxidant, anti-inflammatory and anticancer properties of blackberry and raspberry fruits,” *Journal of Food Composition and Analysis*, vol. 23, no. 6, pp. 554–560, 2010.
- [16] S. Mallakpour and M. Hatami, “Green and eco-friendly route for the synthesis of Ag@Vitamin B9-LDH hybrid and its chitosan nanocomposites:

- Characterization and antibacterial activity,” *Polymer*, vol. 154, pp. 188–199, Jun. 2018, doi: 10.1016/j.polymer.2018.08.077.
- [17] H. Padinjarathil, M. M. Joseph, B. S. Unnikrishnan, G. U. Preethi, R. Shiji, M. G. Archana, S. Maya, H. P. Syama, and T. T. Sreelekha, “Galactomannan endowed biogenic silver nanoparticles exposed enhanced cancer cytotoxicity with excellent biocompatibility,” *International Journal of Biological Macromolecules*, vol. 118, pp. 1174–1182, Jul. 2018, doi: 10.1016/j.ijbiomac.2018.06.194.
- [18] D. Vollath, F. D. Fischer, and D. Fischer, “Surface energy of nanoparticles - influence of particle size and structure,” *Beilstein Journal of Nanotechnology*, vol. 9, no. 1, pp. 2265–2276, Aug. 2018, doi: 10.3762/bjnano.9.211.
- [19] D. Nayak, S. Ashe, P. R. Rauta, M. Kumari, and B. Nayak, “Bark extract mediated green synthesis of silver nanoparticles: Evaluation of antimicrobial activity and antiproliferative response against osteosarcoma,” *Materials Science and Engineering C*, vol. 58, pp. 44–52, 2016, doi: 10.1016/j.msec.2015.08.022.
- [20] N. Hashim, M. Paramasivam, J. S. Tan, D. Kernain, M. H. Hussin, N. Brosse, F. Gambier, and P. BothiRaja, “Green mode synthesis of silver nanoparticles using *Vitis vinifera*’s tannin and screening its antimicrobial activity/apoptotic potential versus cancer cells,” *Materials Today Communications*, vol. 25, Jul. 2020, doi: 10.1016/j.mtcomm.2020.101511.
- [21] W. R. Rolim, M. T. Pelegrino, B. de Araújo Lima, L. S. Ferraz, F. N. Costa, J. S. Bernardes, T. Rodrigues, M. Brocchi, and A. B. Seabra, “Green tea extract mediated biogenic synthesis of silver nanoparticles: Characterization, cytotoxicity evaluation and antibacterial activity,” *Applications of Surface Science*, vol. 463, pp. 66–74, 2019, doi: 10.1016/j.apsusc.2018.08.203.
- [22] J. K. Patra, S. H. Kim, H. Hwang, J. W. Choi, K. Baek, “Volatile compounds and antioxidant capacity of the bio-oil obtained by pyrolysis of Japanese red pine (*Pinus densiflora* Siebold and Zucc.),” *Molecules*, vol. 20, pp. 3986–4006, Mar. 2015, doi: 10.3390/molecules20033986.
- [23] N. J. Reddy, D. Nagoor Vali, M. Rani, and S. S. Rani, “Evaluation of antioxidant, antibacterial and cytotoxic effects of green synthesized silver nanoparticles by *Piper longum* fruit,” *Materials Science and Engineering C*, vol. 34, no. 1, pp. 115–122, 2014, doi: 10.1016/j.msec.2013.08.039.
- [24] T. Campbell, C. Bowen-Forbes, and W. Aalbersberg, “Phytochemistry and biological activity of extracts of the red raspberry *Rubus rosifolius*,” presented at the International Conference on Nutritional and Nutraceutical Sciences, Singapore, Mar. 29–30, 2015.
- [25] Y. Desmiaty, B. Elya, F. C. Saputri, M. Hanafi, and R. Prastiwi, “Antioxidant activity of *Rubus fraxinifolius* Poir. and *Rubus rosifolius* J. Sm. leaves,” *Journal of Young Pharmacists*, vol. 10, no. 2, pp. 93–96, 2018, doi: 10.5530/jyp.2018.2s.18.
- [26] A. Maciolkę and H. Ritter, “One pot synthesis of silver nanoparticles using a cyclodextrin containing polymer as reductant and stabilizer,” *Beilstein Journal of Nanotechnology*, vol. 5, no. 1, pp. 380–385, Mar. 2014, doi:10.3762/bjnano.5.44.
- [27] M. M. Saber, S. B. Mirtajani, and K. Karimzadeh, “Green synthesis of silver nanoparticles using *Trapa natans* extract and their anticancer activity against A431 human skin cancer cells,” *Journal of Drug Delivery Science and Technology*, vol. 47, pp. 375–379, Aug. 2018, doi: 10.1016/j.jddst.2018.08.004.
- [28] L. Biao, S. Tan, X. Zhang, J. Gao, Z. Liu, and Y. Fu, “Synthesis and characterization of proanthocyanidins-functionalized Ag nanoparticles,” *Colloids Surfaces B Biointerfaces*, vol. 169, pp. 438–443, May 2018, doi: 10.1016/j.colsurfb.2018.05.050.
- [29] A. Buccolieri, A. Serra, G. Giancane, and D. Manno, “Colloidal solution of silver nanoparticles for label-free colorimetric sensing of ammonia in aqueous solutions,” *Beilstein Journal of Nanotechnology*, vol. 9, no. 1, pp. 499–507, Feb. 2018, doi: 10.3762/bjnano.9.48.
- [30] S. M. Ghaseminezhad and S. A. Shojaosadati, “Data on the role of starch and ammonia in green synthesis of silver and iron oxide nanoparticles,” *Data in Brief*, vol. 7, pp. 99–103, Mar. 2016, doi: 10.1016/j.carbpol.2016.03.007.
- [31] T. Suwatthanarak, B. Than-Ardna, D. Danwanichakul, and P. Danwanichakul,

- “Synthesis of silver nanoparticles in skim natural rubber latex at room temperature,” *Materials Letters*, vol. 168, pp. 31–35, 2016, doi: 10.1016/j.matlet.2016.01.026.
- [32] L. F. Gorup, E. Longo, E. R. Leite, and E. R. Camargo, “Moderating effect of ammonia on particle growth and stability of quasi-monodisperse silver nanoparticles synthesized by the Turkevich method,” *Journal of Colloid and Interface Science*, vol. 360, no. 2, pp. 355–358, May 2011, doi: 10.1016/j.jcis.2011.04.099.
- [33] I. Ocsoy, A. Demirbas, E. S. McLamore, B. Altinsoy, N. Ildiz, and A. Baldemir, “Green synthesis with incorporated hydrothermal approaches for silver nanoparticles formation and enhanced antimicrobial activity against bacterial and fungal pathogens,” *Journal of Molecular Liquids*, vol. 238, pp. 263–269, May 2017, doi: 10.1016/j.molliq.2017.05.012.
- [34] S. K. Srikar, D. D. Giri, D. B. Pal, P. K. Mishra, and S. N. Upadhyay, “Green synthesis of silver nanoparticles: A review,” *Green and Sustainable Chemistry*, vol. 6, no. 1, Feb. 2016, doi: 10.4236/gsc.2016.61004.
- [35] K. Chitra and G. Annadurai, “Anti-bacterial activity of pH dependent biosynthesized silver nanoparticles against clinical pathogens,” *Biomed Research International*, vol. 2014, no. 725165, May 2014, doi:10.1155/2014/725165.
- [36] P. S. Sadalage, R. V. Patil, M. N. Padvi, and K. D. Pawar, “Almond skin extract mediated optimally biosynthesized antibacterial silver T nanoparticles enable selective and sensitive colorimetric detection of Fe^{+2} ions,” *Colloids and Surfaces B: Biointerfaces*, vol. 193, p. 111084, Apr. 2020, doi: 10.1016/j.colsurfb.2020.111084.
- [37] R. Sattari, G. R. Khayati, and R. Hoshyar, “Biosynthesis and characterization of silver nanoparticles capped by biomolecules by fumaria parviflora extract as green approach and evaluation of their cytotoxicity against human breast cancer MDA-MB-468 cell lines,” *Materials Chemistry and Physics*, vol. 241, p. 122438, 2020, doi: 10.1016/j.matchemphys.2019.122438.
- [38] R. Kalaivani, M. Maruthupandy, T. Muneeswaran, A. H. Beevi, M. Anand, C. M. Ramakritinan, and A. K. Kumaraguru, “Synthesis of chitosan mediated silver nanoparticles (Ag NPs) for potential antimicrobial applications,” *Frontiers in Laboratory Medicine*, vol. 2, no. 1, pp. 30–35, Apr. 2018, doi: 10.1016/j.flm.2018.04.002.
- [39] A. M. Oda, H. Abdulkadhim, S. I. A. Jabuk, R. Hashim, I. Fadhil, D. Alaa, and A. Kareem, “Green synthesis of silver nanoparticle by cauliflower extract: Characterisation and antibacterial activity against storage,” *IET Nanobiotechnology*, vol. 13, no. 5, pp. 1–6, Apr. 2019, doi: 10.1049/iet-nbt.2018.5095.
- [40] E. Tomaszewska, K. Soliwoda, K. Kadziola, B. Tkacz-Szczesna, G. Celichowski, M. Cichomski, W. Szmaja, and J. Grobelny, “Detection limits of DLS and UV-Vis spectroscopy in characterization of polydisperse nanoparticles,” *Journal of Nanomaterials*, vol. 2013, Jun. 2013, doi: 10.1155/2013/313081.
- [41] Nanocomposix, “Zeta potential analysis of nanoparticles,” Nanocomposix, California, USA, Jan. 2020.
- [42] M. Nasirboroumand, M. Montazer, and H. Barani, “Preparation and characterization of biocompatible silver nanoparticles using pomegranate peel extract,” *Journal of Photochemistry and Photobiology B: Biology*, vol. 179, pp. 98–104, Jan. 2018, doi: 10.1016/j.jphotobiol.2018.01.006.
- [43] M. Danaei, M. Dehghankhold, S. Ataei, F. H. Davarani, R. Javanmard, A. Dokhani, S. Khorasani, and M. R. Mozafari, “Impact of particle size and polydispersity index on the clinical applications of lipidic nanocarrier systems,” *Pharmaceutics*, vol. 10, no. 2, pp. 1–17, May 2018, doi: 10.3390/pharmaceutics10020057.
- [44] M. Zia, S. Gul, J. Akhtar, I. Ul Haq, B. H. Abbasi, A. Hussain, S. Naz, and M. F. Chaudhary, “Green synthesis of silver nanoparticles from grape and tomato juices and evaluation of biological activities,” *IET Nanobiotechnology*, vol. 11, no. 2, pp. 193–199, 2017, doi: 10.1049/iet-nbt.2015.0099.
- [45] E. Dogru, A. Demirbas, B. Altinsoy, F. Duman, and I. Ocsoy, “Formation of *Matricaria chamomilla* extract-incorporated Ag nanoparticles and size-dependent enhanced antimicrobial property,” *Journal of Photochemistry and Photobiology B: Biology*, vol. 174, pp. 78–83, Jul. 2017, doi: 10.1016/j.jphotobiol.2017.07.024.
- [46] A. Virgen-Ortiz, S. Limón-Miranda, M. A. Soto-Covarrubias, A. Apolinar-Irbe, E. Rodríguez-

- León, and R. Iñiguez-Palomares, “Biocompatible silver nanoparticles synthesized using *Rumex hymenosepalus* extract decreases fasting glucose levels in diabetic rats,” *Digest Journal of Nanomaterials and Biostructures*, vol. 10, no. 3, pp. 927–933, Sep. 2015.
- [47] S. M. Magaña, P. Quintana, D. H. Aguilar, J. A. Toledo, C. Ángeles-Chávez, M. A. Cortés, L. León, Y. Freile-Pelegrín, T. López, and R. M. T. Sánchez, “Antibacterial activity of montmorillonites modified with silver,” *Journal of Molecular Catalysis A: Chemical*, vol. 281, no. 1–2, pp. 192–199, 2008, doi:10.1016/j.molcata.2007.10.024.
- [48] R. A. Hamouda, M. H. Hussein, R. A. Abo-elmagd, and S. S. Bawazir, “Synthesis and biological characterization of silver nanoparticles derived from the cyanobacterium *Oscillatoria limnetica*,” *Scientific Reports*, vol. 9, no. 1, pp. 1–17, Sep. 2019, doi: 10.1038/s41598-019-49444-y.
- [49] A. Pawlak and M. Mucha, “Thermogravimetric and FTIR studies of chitosan blends,” *Thermochimica Acta*, vol. 396, pp. 153–166, Feb. 2003, doi: 10.1016/S0040-6031(02)00523-3.
- [50] B. Kumar, K. Smita, L. Cumbal, and A. Debut. “Green synthesis of silver nanoparticles using Andean blackberry fruit extract,” *Saudi Journal of Biological Sciences*, vol. 24, no. 1, pp. 45–50, 2017, doi: 10.1016/j.sjbs.2015.09.006.
- [51] N. D. A. Krupa and V. Raghavan, “Biosynthesis of silver nanoparticles using aegle marmelos (Bael) fruit extract and its application to prevent adhesion of bacteria: A strategy to control microfouling,” *Bioinorganic Chemistry and Applications*, vol. 2014, Sep. 2014, doi: 10.1155/2014/94958.
- [52] M. Behravan, A. H. Panahi, A. Naghizadeh, M. Ziaee, R. Mahdavi, and A. Mirzapour, “Facile green synthesis of silver nanoparticles using *Berberis vulgaris* leaf and root aqueous extract and its antibacterial activity,” *International Journal of Biological Macromolecules*, vol. 124, pp. 148–154, 2019, doi: 10.1016/j.ijbiomac.2018.11.101.
- [53] S. L. Hitesh, “Green chemistry based synthesis of silver nanoparticles from floral extract of *Nelumbo nucifera*,” *Materials Today: Proceedings*, vol. 5, no. 2, pp. 6227–6233, 2018, doi: 10.1016/j.matpr.2017.12.231.
- [54] B. Kumar, K. Smita, L. Cumbal, and A. Debut, “Green synthesis of silver nanoparticles using Andean blackberry fruit extract,” *Saudi Journal of Biological Sciences*, vol. 24, no. 1, pp. 45–50, Jan. 2017, doi: 10.1016/j.sjbs.2015.09.006.
- [55] A. Demirbas, V. Yilmaz, N. Ildiz, A. Baldemir, and I. Ocsoy, “Anthocyanins-rich berry extracts directed formation of Ag NPs with the investigation of their antioxidant and antimicrobial activities,” *Journal of Molecular Liquids*, vol. 248, pp. 1044–1049, Oct. 2017, doi: 10.1016/j.molliq.2017.10.130.
- [56] F. S. AlQahtani, M. M. AlShebly, M. Govindarajan, S. Senthilmurugan, P. Vijayan, and G. Benelli, “Green and facile biosynthesis of silver nanocomposites using the aqueous extract of *Rubus ellipticus* leaves: Toxicity and oviposition deterrent activity against Zika virus, malaria and filariasis mosquito vectors,” *Journal of Asia-Pacific Entomology*, vol. 20, pp. 157–164, 2017, doi: 10.1016/j.aspen.2016.12.004.